

Shock Compression of Hydrogen and Other Small Molecules

W.J. Nellis

This article was submitted to
International School of Physics "Enrico Fermi" Course on "High
Pressure Phenomena", Varenna, Italy, July 3-13, 2001

July 6, 2001

U.S. Department of Energy

Lawrence
Livermore
National
Laboratory

DISCLAIMER

This document was prepared as an account of work sponsored by an agency of the United States Government. Neither the United States Government nor the University of California nor any of their employees, makes any warranty, express or implied, or assumes any legal liability or responsibility for the accuracy, completeness, or usefulness of any information, apparatus, product, or process disclosed, or represents that its use would not infringe privately owned rights. Reference herein to any specific commercial product, process, or service by trade name, trademark, manufacturer, or otherwise, does not necessarily constitute or imply its endorsement, recommendation, or favoring by the United States Government or the University of California. The views and opinions of authors expressed herein do not necessarily state or reflect those of the United States Government or the University of California, and shall not be used for advertising or product endorsement purposes.

This is a preprint of a paper intended for publication in a journal or proceedings. Since changes may be made before publication, this preprint is made available with the understanding that it will not be cited or reproduced without the permission of the author.

This report has been reproduced directly from the best available copy.

Available electronically at <http://www.doc.gov/bridge>

Available for a processing fee to U.S. Department of Energy
And its contractors in paper from
U.S. Department of Energy
Office of Scientific and Technical Information
P.O. Box 62
Oak Ridge, TN 37831-0062
Telephone: (865) 576-8401
Facsimile: (865) 576-5728
E-mail: reports@adonis.osti.gov

Available for the sale to the public from
U.S. Department of Commerce
National Technical Information Service
5285 Port Royal Road
Springfield, VA 22161
Telephone: (800) 553-6847
Facsimile: (703) 605-6900
E-mail: orders@ntis.fedworld.gov
Online ordering: <http://www.ntis.gov/ordering.htm>

OR

Lawrence Livermore National Laboratory
Technical Information Department's Digital Library
<http://www.llnl.gov/tid/Library.html>

Shock Compression of Hydrogen and Other Small Molecules

W. J. Nellis

University of California
Lawrence Livermore National Laboratory
Livermore, California 94550

I. Introduction

Hydrogen at high pressures has been a major scientific issue ever since Wigner and Huntington predicted that solid hydrogen would undergo molecular dissociation to a monatomic solid at a pressure P of ~ 25 GPa (250 kbar) at temperature $T = 0$ K. Since a monatomic solid has a half-filled band, it is a metal. Thus, pressure induced dissociation of molecular hydrogen induces an insulator-metal transition [1]. This Wigner transition is yet to be observed. In addition, because Jupiter is composed of ~ 90 at. % hydrogen, the convective dynamo action of metallic fluid hydrogen at high pressures and modest temperatures causes the magnetic field of Jupiter [2]. Thus, understanding hydrogen metallization is essential for understanding how the large magnetic field is generated in the deep Jovian interior. Hydrogen has recently been observed to be metallic at 140 GPa, ninefold compressed initial liquid density, and 2600 K achieved in the fluid with a reverberating shock wave [3]. This nonmetal-metal transition is a Mott transition [4] and is responsible for the Jovian magnetic field [5]. For hydrogen 2600 K is a modest temperature because it is small compared to the Fermi temperature T_F of the metal and comparable to the ground state vibrational energy of the diatomic molecule.

Despite the fact that cold dense hydrogen ($Z=1$) is expected to be well understood, it is not. The theory of dense hydrogen at 0 K is quite difficult because of its large zero-point motions and lack of core electrons. As a result, the predicted metallization pressure at $T=0$ K has ranged from 25 to 2000 GPa [1,6]. Hydrogen is not metallic up to 340 GPa in the room-temperature solid [7-9]. Current estimates put the metallization pressure within the molecular solid phase above 430 GPa using LDA theory [10], which is roughly comparable with the estimate of ~ 620 GPa for the Wigner transition based on extrapolation of static high pressure data up to 120 GPa [11]. The wide range of unobserved predicted

metallization pressures indicates that hydrogen experiments are essential.

The fact that fluid hydrogen is metallic illustrates the importance of modest temperatures at high pressures in the condense phase; i. e., in the regime $T_M < T \ll T_F$, where T_M is the melting temperature. Ultrahigh pressures of several 100 GPa are achieved statically in hydrogen with a diamond-anvil cell. However, if the cell is heated statically even a few 100 K, hydrogen rapidly diffuses out of the cell before a measurement can be made [12]. On the other hand the lifetime of the shock experiment is ~ 100 ns, long for thermal equilibrium and too short to loose hydrogen by mass diffusion and chemical reactions with the sample holder. Thus, dynamic compression with a reverberating shock wave is an ideal way for studying dense fluid hydrogen at both high pressures and modest temperatures, conditions in hydrogen yet to be achieved by other means.

It is the modest temperatures which enable observation of a metallic phase. The value of the conductivity of metallic hydrogen is $2000/\Omega\text{-cm}$, which is the minimum conductivity of a disordered metal. In this case the mean free path of an electron is essentially the distance between adjacent atoms or molecules supplying conduction electrons [13]. The calculated temperatures are about twice the calculated melting temperatures at the pressures in the experiments. Hence, the thermodynamic states are expected to be in the metallic fluid phase, which is expected to have the minimum conductivity of a metal, as observed. So disorder induced by melting at the appropriate density is crucial to being able to observe a metallic state and melting is induced by appropriate temperatures achieved with a reverberating shock wave.

Pressures of 90-180 GPa and temperatures of 1700-3100 K were achieved with a reverberating shock wave generated with a two-stage light-gas gun [3,14,15]. The samples of liquid H_2 or D_2 at 20 K were 25 mm in diameter and 0.5 mm thick. The electrodes were 0.75 mm in diameter separated by 1.5 mm. These relatively large dimensions could be used because the extreme conditions were generated by an impactor 25 mm in diameter and because the experiments were done under inertial confinement, that is, the experiment is over when the compressive shock wave reaches a free surface of the sample holder. Thus, the sample holder need not support high pressures but only accommodate the initial conditions near atmospheric pressure and 20 K.

These shock-reverberation experiments have four significant advantages: (i) the lifetime of the experiment (~ 100 ns) is short for mass diffusion and long for thermodynamic equilibrium, (ii) the temperatures

are relatively high (2000-4000 K) so that (iii) hydrogen is melted and disordered and (iv) sample and electrode diameters are relatively large (25 and 0.75 mm, respectively) which means sample holders are straightforward to fabricate and shielding of electrical noise in the voltage measurement is straightforward.

Electrical conductivities of hydrogen have also been measured under single-shock (Hugoniot) compression up to 20 GPa and 4600 K [16]. Those measurements showed that electronic conduction is thermally activated in the semiconducting fluid. Hugoniot equation-of-state (EOS) and shock temperatures have also been measured for hydrogen under single and double-shock compression [17,18]. Those data have been used to generate a scaling relationship for the electrical conductivity of hydrogen as a function of density and temperature at high pressures [5].

The model to explain the onset of metallic conduction in dense fluid hydrogen is not specific to hydrogen. Hence, other simple diatomic fluids are expected to undergo a Mott transition as well. To test this hypothesis, oxygen was investigated up to 180 GPa and observed to reach minimum metallic conductivity at a pressure predicted for a Mott transition [19], as expected. Nitrogen undergoes a Mott transition at the predicted pressure, as well [20]. On the other hand, it is important to find a hydrogen-rich fluid that does not become a metal at 100 GPa pressures in the fluid. Water is a hydrogen-rich fluid which is a proton conductor, rather than a metal, under compression up to 180 GPa by a reverberating shock wave, as expected [21]. Once the electrical conductivities of dense fluid hydrogen became known [5], it became possible to test the hypothesis that hydrocarbons decompose into diamond-like C and H₂ at high shock pressures [22]. For this reason electrical conductivities of methane (CH₄) and benzene (C₆H₆), which were measured fifteen years ago, were recently analyzed. The results suggest that these hydrocarbons do decompose into diamond-like C nanoparticles and H₂ at high shock pressures [23].

Our purpose here is to describe dynamic experiments to compress and diagnose low-Z fluids at extreme conditions up to 200 GPa achieved with a two-stage light-gas gun and to describe nonmetal-metal transitions in dense fluid hydrogen and oxygen, proton conduction in water which is essentially totally ionized, and chemical decomposition of the hydrocarbons methane and benzene.

II. Finite Temperatures

Because shock compression is fast, it is adiabatic and temperature increases. By "fast" we mean that the lifetime of the experiment is short compared to the time required for thermal transport out of the sample into the surrounding medium. The amount temperature increases is determined by the rate at which pressure is applied. By controlling temperature, thermal pressure is controlled and, so is density. **Fig.1** illustrates the effect of pressure rise time on thermodynamic states achieved dynamically in dense hydrogen. **Fig. 1a** shows two extreme cases in which pressure increases instantaneously in one sharp step (or shock) to final pressure and the case in which pressure increases in ~10 sharp steps to the same final pressure; **Fig. 1b** illustrates that a single-step (or Hugoniot) compression produces very high temperatures and thermal pressures, which result in a modest maximum density, while the multi-step process produces much lower temperatures and thermal pressures and substantially higher densities relatively close to the 0-K isotherm. The multistep process was achieved experimentally with a shock wave reverberating in hydrogen between two stiff anvils.

III. Minimum Metallic Conductivity: Hydrogen

These experiments were performed at conditions at which metallization is driven by density and the temperature is just sufficient to cause melting to the disordered fluid. These conditions are achieved with a two-stage light-gas gun.

A. Experiment

A liquid layer of H₂ or D₂ 0.5 mm thick and 25 mm in diameter at 20 K was compressed by a shock wave reverberating between two stiff, electrically insulating sapphire anvils (single-crystal Al₂O₃) 2.0 mm thick and 25 mm in diameter. These sapphire disks are contained between two 2.0 mm-thick Al (alloy 1100) disks of the main body of the Al cryogenic target assembly. Al is strong, ductile, and a good thermal conductor at 20 K, which facilitates condensing the sample from high-purity gas. The hydrogen layer thickness was chosen such that the experiment would have a sufficiently short time duration that deleterious effects could not occur (loss of the high-temperature hydrogen by mass diffusion and chemical

reactions), while being sufficiently long to achieve thermal and electrical equilibrium.

The compression is initiated by a strong impact-generated shock incident from one of the anvils into the liquid hydrogen. Electrical resistance of the hydrogen sample is measured versus time by inserting electrodes (302 stainless steel) through the other anvil, as illustrated in **Fig. 2a**. The incident shock was produced by impact of a planar metal plate accelerated up to ~ 7 km/s with a two-stage light-gas gun [14]. The 25 mm-diameter impactor consisted either of an Al or Cu plate 3.0 mm thick, hot-pressed into a Lexan polycarbonate sabot.

In order for the hydrogen sample to achieve the highest densities and lowest temperatures at high pressures, the sample must have a relatively high initial density. High initial density was achieved by using a liquid sample near the saturation curve. Either H_2 or D_2 samples were used, depending on the final density and temperature desired. That is, because the initial mass densities of liquid H_2 and D_2 at 20 K differ by a factor of 2.4, their final shock-compressed densities, temperatures, and conductivities also differ substantially at the same final pressure. Thus, the two isotopes are used to achieve different thermodynamic states, rather than to look for an isotope effect. Since the sample holder is destroyed by the impact shock, a new cryogenic one is required for each experiment.

The electrical circuit for four-probe measurements is shown in **Fig. 2b**. All cables are coaxial. Voltage histories were measured with Tektronix DSA 602A digital oscilloscopes and 7103 analogue oscilloscopes with ~ 2 ns time resolution, triggered at the appropriate time. In order to measure relatively low potential differences in a noisy environment, the oscilloscopes were used in a differential mode; i. e., voltage was measured on each probe relative to ground and then voltage difference was determined to eliminate common electrical noise on both cables. The current was measured with a Rowgowski coil. Typical currents were ~ 1 A and voltages were a few tens of mV. The current density in the hydrogen sample was ~ 500 A/cm² for 100 ns. Electrical resistivity ρ was derived from measured electrical resistance R through the cell constant C : $R = C\rho$. Cell constant C was determined by experimental calibration and/or computational simulation.

The measured electrical resistivity of shock-compressed sapphire [24] is five orders of magnitude larger than that of

hydrogen at metallization, which means that sapphire is effectively an electrical insulator in these experiments. The electrically insulating nature of Al_2O_3 at 100 GPa dynamic pressures is not affected by the fact that Al_2O_3 undergoes a slow diffusive phase transition at ~ 100 GPa static pressures and ~ 1000 K [25].

Logarithms of measured electrical resistivities $\log(\rho)$ are plotted versus pressure P in **Fig. 3**. P is final shock reverberation pressure P_f in **Fig. 4**. These data are tabulated elsewhere [14].

Similar results have been obtained with shock compression driven by high explosives [26].

B. Thermodynamic States

The shock reverberation for our experiment at 180 GPa is illustrated in **Fig. 4a**, plotted as pressure P versus mass velocity u_p behind a shock front. That is, a shock wave travels at a supersonic velocity u_s , which causes mass behind the shock front to move in the same direction at mass velocity u_p . P and u_p are continuous across an interface. In **Fig. 4b** the dependence on time t of pressure at the midpoint of the hydrogen layer is shown. The values of the pressure steps are caused by the shock reverberating in hydrogen between the two stiff sapphire disks. The values of P , u_p , and t in **Fig. 4** were obtained by computational simulation [27].

The impact causes an initial pressure P_f in the Al_2O_3 . When this shock reaches the liquid hydrogen, the pressure drops until the release pressure of sapphire matches the Hugoniot of liquid hydrogen (state 1 in **Fig. 4**). This drop is about a factor of 30 in pressure. The shock in hydrogen then reverberates back and forth between the sapphire anvils until the pressure reaches P_f , the pressure incident initially from the sapphire. For a typical initial 5 GPa shock in hydrogen, the pressure increases a factor of 50,000 from ambient, which causes some shock heating. However, the successive reverberations are very weak shocks because the pressure increases only a factor of 4 or less on each of these reflections. Thus, the total of all the shock reflections off sapphire corresponds to a quasi-isentrope. This fast compression process is adiabatic and the hydrogen is heated. About 40% of the final temperature is caused by the first shock and the remainder by the quasi-isentrope. The pressure-density states achieved are on the solid curve in **Fig. 1b**.

Shock reverberation is necessary to reach metallization near 0.7 g/cm.³ The various pressure-density curves in **Fig. 1b** were calculated using the equation of state of Kerley [28].

The densities and temperatures must be known to analyze the electrical conductivities. At present these must be calculated because it is not yet known how to measure them. Densities and temperatures were calculated by computationally simulating the experiments with two representative hydrogen EOSs of Kerley and Ross [28,29]. Based on the differences between these calculations, the systematic uncertainties in calculated density and temperature are 6% and 30%, respectively, more than sufficient to justify the occurrence of a nonmetal-metal transition.

C. Semiconducting Fluid Hydrogen

The change of slope at 140 GPa in Fig. 3 is the nonmetal-metal transition. At pressures of 90 to 140 GPa fluid hydrogen is semiconducting. When plotted versus pressure, $\log(\rho)$ for both hydrogen and deuterium fall on the same curve because density and temperature increase monotonically with pressure for both isotopes [14]. Data in the semiconducting regime 93-120 GPa fit the relationship

$$\sigma = \sigma_0 \exp (- E_g(D) / 2k_B T), \quad (1)$$

where σ is electrical conductivity, σ_0 depends on density D , $E_g(D)$ is the density-dependent mobility gap in the electronic density of states of the fluid, k_B is Boltzmann's constant, and T is temperature. Six data points were fit to Eq. (1). Densities of these points varied from 0.291 to 0.326 mol H₂/cm³ and temperature was in the range 2100 to 2800 K. The densities and temperatures calculated with Ross' model were used for the fit to Eq. (1). The conductivity values calculated from this fit differ from the measured values within the magnitude of the error bars. The results of this least-squares fit are:

$$E_g(D) = 1.22 - (62.6)(D - 0.30), \quad (2)$$

where $E_g(D)$ is in eV, D is in mol H_2/cm^3 (0.29-0.32), and $\sigma_0 = 90 (\Omega\text{-cm})^{-1}$.

The $E_g(D)$ derived from this fitting procedure and $k_B T$ are equal at a density of 0.32 mol H_2/cm^3 and a temperature of ~ 2600 K (0.22 eV), as illustrated in **Fig. 5**. In this region, the energy gap is smeared out thermally, activation of electron carriers is complete, disorder is saturated in the fluid, and conductivity is expected to be weakly sensitive to further increases in pressure and temperature, provided the nature of the fluid does not change significantly. At 0.32 mol H_2/cm^3 the calculated pressure is 120 GPa, which is close to the 140 GPa pressure at which the slope changes in the electrical resistivity (**Fig. 3**). The 10% increase in density from 0.29-0.32 mol H_2/cm^3 causes the bandgap to decrease from 1.8 eV to ~ 0.25 eV, where the gap is filled in by fluid disorder and thermal smearing. Thus, fluid hydrogen becomes metallic at about 140 GPa and ~ 2600 K via a continuous transition from a semiconducting to metallic fluid. Because conductivities are thermally activated in the semiconducting regime [14,16], electronic states at the Fermi level of this disordered material are localized.

Because densities were not measured, it is not yet possible to know experimentally if a density discontinuity occurs at metallization. Nevertheless, it is our opinion that because of the high densities and temperatures and lack of a clear resistivity discontinuity in **Fig. 3**, a density discontinuity does not occur at metallization.

D. Metallic Fluid Hydrogen

Since these experiments are at finite temperatures in the disordered fluid, the density of electron states (DOS) around the Fermi level is not zero, as for a crystalline semiconductor at $T = 0$ K. Thermal smearing and disorder cause a small, nonzero DOS near the Fermi level in semiconducting fluid hydrogen [30]. Increasing pressure reduces the 15 eV bandgap and thermal disorder fills it in. When pressure and temperature are such that $E_g/k_B = T \sim 2600$ K, the depression in the bandgap is filled in, a metallic density of states is achieved, and the electronic system has a Fermi surface characteristic of a metal.

Characteristic energies are plotted versus density in **Fig. 5**. E_{gap} produced by single-shock compression [16] is the point at 0.13 mol H_2/cm^3 . The linear dependence of E_{gap} near 0.3 mol H_2/cm^3 was determined in multiple-shock experiments (Eq. (2)). These two determinations are interpolated linearly by the dashed line. The molecular dissociation energy E_{diss} was extrapolated from Ross' model [18]. The calculated temperatures in these conductivity experiments are also shown plotted as $k_{\text{B}}T$. **Fig. 5** shows that the temperatures are relatively low compared to E_{gap} and E_{diss} and that these conductivity experiments are sensitive primarily to electronic excitation, with a relatively small amount of molecular dissociation. This is consistent with the suggestion that conduction in dense hydrogen is caused by electrons delocalized from H_2 molecules, which causes H_2^+ ions [31]. The free H_2^+ ion is quite stable, having a dissociation energy of 2.8 eV, and thus it is reasonable to expect them to exist at these conditions. Further discussion follows below about whether metallic fluid hydrogen should be considered to be monomeric or dimeric.

Tight-binding molecular dynamics calculations of Lenosky et al [30] also show that fluid metallic hydrogen at 3000 K is "molecular" on a very short time scale. These simulations show a peak in the proton-proton pair distribution function at a distance corresponding to the separation between protons in the molecule. A relatively low dissociation fraction of H_2 was estimated at $r_s = 1.54$ (0.37 mol/ cm^3) and 3000 K, which is in the metallic range. At lower densities of 0.17 mol/ cm^3 at 3000 K, this disordered semiconducting fluid is composed of a mixture of molecules and a few percent of atoms. A depression exists in the DOS around the Fermi level. About half of the relatively few states at the Fermi level come from diatomic molecules and half from atoms, both of which occupy a common energy band.

These MD simulations also show that "molecules" are short-lived (10^{-14} to 10^{-13} s). A proton pair exists for a few molecular vibrational periods and then on subsequent collision breakups into atoms, which combine with other atoms to form new dimers or remain unpaired as atoms, and so forth. Because of the short lifetimes, a better term to describe such an object is "transient pair." It is also reasonable to assume that a particular electron might bind two protons into one H_2^+ transient pair and then be the

conduction electron in its next transient pair. Other species, such as H_2^+ , H_2 , H^+ , H , H_3^+ , and possibly higher order H clusters might be present as well. These MD simulations also show that kinetic, vibrational, and rotational energies of the transient pairs are comparable and dissociation commences at conditions near those for the onset of metallization.

In this tight-binding picture conduction electrons have a very short mean free path, namely, the distance between adjacent particles supplying conduction electrons. A conducting electron exchanges with its neighbor when electronic overlap is sufficiently large to allow an electron to hop to its nearest neighbor to produce a net current flow. This is a strong-scattering system and describes a state characteristic of the minimum conductivity of a metal.

Metallic fluid hydrogen is highly degenerate because of the very high density of electrons. At a molar density of $0.32 \text{ mol H}_2/\text{cm}^3$ the Fermi energy is 19 eV and $T/T_F \sim 0.01$.

The fluids Cs, Rb, and hydrogen at $\sim 2000 \text{ K}$ all metallize with the same electrical conductivity of $2000 (\Omega\text{-cm})^{-1}$ [32]. These fluids also obey the same condition of metallization, namely, the same scaled density $= D_m^{1/3} a^*$, where D_m is the number density of conduction electrons and a^* is the effective Bohr radius. This scaled density is simply the ratio of two length scales, namely, the ratio of the size of the free particle, a^* , to the average distance between particles at metallization, $D_m^{-1/3}$. This transition to the metallic fluid occurs at the same value of $D_m^{1/3} a^* = 0.38$ for fluids Cs, Rb, and H. Since the Bohr radii of H and H_2 are essentially equal [14], the scaled electron densities for monatomic and diatomic hydrogen differ simply by the factor $2^{1/3}$. Thus, for pure H_2 , metallization occurs at $D_m^{1/3} a^* = 0.30$. The value of $D_m^{1/3} a^*$ is not very sensitive to whether hydrogen is diatomic or monatomic.

E. Density at Metallization

The density of metallization, $0.32 \text{ mol H}_2/\text{cm}^3$, was derived by computational simulation of all the experiments to calculate densities and temperatures. Conductivities in the semiconducting phase were then fit as a function of density and temperature to Eq. (1). Metallization density is taken as the density at which the volume-dependent mobility gap equals $\sim k_B T$. The species was

assumed to be primarily H_2 because temperatures are comparable to the ground state vibrational energy of the hydrogen molecule, phenomenological theory indicates a high concentration of molecules rather than atoms [18], and quantum simulations suggest that a substantial concentration of dimers live for a lifetime of the order of the vibrational period of the free molecule, $\sim 10^{-14}$ s [30].

On the other hand, metallization density is given by the Goldhammer-Herzfeld criterion [33], which depends only on the polarization of the free particle. Using the polarization of the free hydrogen atom gives a metallization density of 0.595 mol H/cm^3 , which is within 7 % of the metallization density of $0.32 \text{ mol H}_2/\text{cm}^3 = 0.64 \text{ mol H/cm}^3$ determined by the method in the previous paragraph. While the good agreement between the two values of metallization density might be fortuitous, this agreement does suggest that fluid metallic hydrogen might be monomeric. That is, since time resolution of the diagnostic system of the conductivity experiments is 10^{-9} s, dimer lifetimes of 10^{-14} s [30] are not possible to detect, and so the system looks monomeric within the time resolution.

F. Minimum Conductivity of a Metal

The Drude conductivity, σ , is given by:

$$\sigma = n e^2 \tau / m, \quad (3)$$

where n is the number of conduction electrons per unit volume, e and m are the charge and mass of the electron, respectively, and τ is the relaxation time for electron scattering. In a strong-scattering system the relaxation time is given by the Ioffe-Regel [34] condition $\tau = d/v_F$, where d is the electron mean free path, equal to the average nearest-neighbor distance, and v_F is the Fermi velocity. In this case Eq. (3) reduces to [13]

$$\sigma_{\min} = 2\pi e^2 / (3hd), \quad (4)$$

where h is Planck's constant, and $d = D_m^{-1/3}$. For a metallization density of 0.595 mol H/cm^3 obtained from the Herzfeld criterion,

$\sigma_{\min} = 6000 \text{ } (\Omega\text{-cm})^{-1}$, which is in good agreement with the measured value of $2000 \text{ } (\Omega\text{-cm})^{-1}$. Under the extreme assumption that H_2 molecules are stable and a metallization volume of $0.32 \text{ mol H}_2/\text{cm}^3$, Eq. (4) gives a conductivity of $5000 \text{ } (\Omega\text{-cm})^{-1}$. Since the values of metallization volume and conductivities are similar under the assumption that hydrogen is monatomic or diatomic, existing conductivity data cannot distinguish between the two. Metallic conductivity values in good agreement with experiment were calculated by Louis and Ashcroft with the Ziman model [35] for molecular hydrogen and with tight-binding molecular dynamics [36] which indicate that dimers are short-lived. The latter show that the nonmetal-metal transition in hydrogen is density-driven at conditions in these experiments; that is, once sufficient density is achieved, metallic conductivity depends weakly on temperature in the disordered fluid.

IV. Nonmetallic Fluid Hydrogen

Nonmetallic fluid hydrogen is achieved by single and double-shocking liquid hydrogen or deuterium samples. Basic shock-compression phenomenology is described elsewhere in these proceedings [37]. Since shock pressure is proportional to initial mass density, hydrogen and deuterium samples are used to generate different pressures, densities, and temperatures. Hugoniot (EOS) pressure-volume experiments, shock temperature experiments, and electrical conductivity experiments are illustrated in Fig. 6. In EOS experiments shock velocity is measured with point detectors either in the liquid sample to characterize the first shock-compressed state or across an anvil against which the first shock is reflected. Temperature is measured from the spectral dependence of optical radiation from the front of the first shock or from the interface of double-shocked deuterium and a transparent crystal anvil. The thermal emission spectrum is fit to a gray body spectrum which has a characteristic emission temperature. Electrical resistance is measured by inserting two planar electrodes of a size $\sim 1.0 \times 1.0 \times 0.05 \text{ mm}^3$ into the liquid and measuring voltage and current versus time as the first shock traverses the electrodes. Resistance R is converted to resistivity ρ via the cell constant C : $R = C\rho$. C is determined by experimental calibration and/or computation.

Figure 7 shows on the left single and double-shocked Hugoniot EOS data for liquid deuterium [17] and on the right double-shock temperature data for liquid deuterium [18]. Maximum double-shock conditions are a pressure of 80 GPa, a volume of $4 \text{ cm}^3/\text{mol}$ which is sixfold compressed liquid, and a temperature of 5000 K. The Present model is [18]; RRY is [38]. Electrical conductivities of deuterium shock-compressed from 13.3 to 20.4 GPa are shown in Fig. 8 [16]. The temperatures in these conductivity experiments range from 2900 to 4600 K. The data in Fig. 8 have an activation energy of 11.7 eV at $7.5 \text{ cm}^3/\text{mol}$.

V. Minimum Metallic Conductivity: Oxygen and Nitrogen

The model to explain the minimum metallic conductivity of fluid hydrogen is not specific to hydrogen. Thus, this model should apply to the similar diatomic fluids, oxygen and nitrogen, as well. That is, since minimum metallic conductivity is weakly dependent on material (Eq. (4)), a conductivity of $\sim 1000 (\Omega\text{-cm})^{-1}$ is expected for both oxygen and nitrogen. In addition, this conductivity should occur at a pressure which induces a Mott transition. These features are observed in the electrical conductivities of both oxygen [19] and nitrogen [20] at 100 GPa pressures. The results for oxygen are shown in Fig. 9, a plot of $\log(\sigma)$ versus Mott scaling parameter.

VI. Proton Conductivity: Water

It is important to find an H-rich fluid which does not become metallic at 100 GPa pressures in the experiment in Fig. 2. Measurements of the electrical conductivity of water up to 60 GPa on the Hugoniot [39] were explained quantitatively by assuming that conduction is caused by one proton per compressed molecule and that proton scattering relaxation time is the distance between adjacent molecules divided by classical thermal velocity. Since the maximum number of protons are produced by single-shock compression at 60 GPa, then going to a pressure of 200 GPa with shock reverberation is not expected to have a significantly higher conductivity. To test this idea, the electrical conductivity of water was measured in the range 70 to 180 GPa and temperatures of 4,000 to 10,000 K [40]. The measured conductivities are in the range 40 to 200 $(\Omega\text{-cm})^{-1}$.

This relatively weak pressure dependence is consistent with water being fully ionized chemically and protons being the dominant conduction mechanism. These results are illustrated in Fig. 10, which includes results from previous water conductivity measurements under single-shock compression along the Hugoniot [39,41]. Measured conductivities in the range 50 to 180 GPa are in agreement with recent Quantum Molecular Dynamics calculations which indicate that protons are the dominant charge carriers [42].

VI. Hydrocarbons: Chemical Decomposition

Because the electrical conductivities of dense fluid hydrogen [5] and of graphite shocked into the diamond phase [43] are now known, it has become possible to test the hypothesis that hydrocarbons decompose into diamond-like C and H₂ at high shock pressures [22]. For this reason electrical conductivities of methane (CH₄) and benzene (C₆H₆) were recently analyzed. The results suggest that these hydrocarbons do decompose into diamond-like C nanoparticles and H₂ at high shock pressures [23].

Conductivities were measured for methane and benzene singly shocked to pressures in the range 20 to 60 GPa and temperatures in the range 2000 to 4000 K achieved with a two-stage light-gas gun. The data for methane and benzene can be interpreted simply in terms of chemical decomposition into diamond-like, defected C nanoparticles and fluid H₂ and their relative abundances (C:H₂), 1:2 for methane and 2:1 for benzene. Conduction is predominately through the majority species.

Conductivity data for methane are plotted as the crosses in Fig. 11 versus single-shock pressure. For comparison, the dashed line represents conductivities expected if methane decomposed completely into diamond-like C and H₂. At 26 GPa methane conductivity is two orders of magnitude lower than expected if it decomposed, which suggests methane is still molecular. On the other hand, at 36 GPa methane conductivity is within a factor of 3 of what is expected if methane decomposed completely into diamond-like C and H₂, which suggests that methane has decomposed substantially. These results suggest that methane is in a range of Hugoniot shock pressures in which dissociation increases

continuously from a system which is mostly methane near 26 GPa to one which has a substantial concentration of H₂ near 36 GPa.

Conductivity data for benzene are plotted versus single-shock pressure in Fig. 12. Exponential increase of benzene conductivities at 20-40 GPa is probably caused by thermal activation of nucleation, growth, and connectivity of diamond-like, defected C nanoparticles following decomposition of benzene. At 40 GPa the concentration of these C nanoparticles reaches a critical density, such that further increase in their density does not have a significant affect on the cross sectional area of conduction and, thus, conductivity saturates. The value of conductivity on the plateau above 40 GPa is 40 ($\Omega\text{-cm}$)⁻¹, essentially the same value of graphite shock-compressed into the diamond phase [43], which suggests conduction is predominantly through defected diamond-like C.

ACKNOWLEDGMENTS

This work was performed under the auspices of U.S. Department of Energy by the University of California Lawrence Livermore National Laboratory under Contract No. W-7405-ENG-48.

References

- [1] WIGNER E. and HUNTINGTON H. B., *J. Chem. Phys.*, **3** (1935) 764.
- [2] STEVENSON, D. J., *Rep. Prog. Phys.*, **46** (1983) 555.
- [3] WEIR S. T., MITCHELL A. C., and NELLIS W. J., *Phys. Rev. Lett.*, **76** (1996) 1860.
- [4] MOTT N. F. and DAVIS E. A., *Electronic Processes in Non-Crystalline Materials* (Oxford Press, London) 1971, p. 133.
- [5] NELLIS W. J., WEIR S. T., and MITCHELL A. C., *Science* **273**, (1996) 936.
- [6] ALDER B. J. and CHRISTIAN R. H., *Phys. Rev. Lett.*, **4** (1960) 450.
- [7] CHEN H. N., STERER E., and SILVERA I. F., *Phys. Rev. Lett.* **76** (1996) 1663.
- [8] HEMLEY R. J., MAO H. K., GONCHAROV A. F., HANFLAND M., and STRUZHKIN V., *Phys. Rev. Lett.*, **76** (1996) 1667.
- [9] NARAYANA C., LUO H., ORLOFF J., and RUOFF A. L., *Nature* **393** (1998) 46.
- [10] ASHCROFT N. W. and JOHNSON K. A., *Nature*, **403** (2000) 632.
- [11] LOUBEYRE P. et al, *Nature*, **383** (1996) 702.
- [12] DATCHI F., LOUBEYRE P., and LETOULLEC R., *Phys. Rev. B*, **61** (2000) 6535.
- [13] MOTT N. F. and DAVIS E. A., *Electronic Processes in Non-Crystalline Materials* (Oxford Press, London) 1971, p. 81.
- [14] NELLIS W. J., WEIR S. T., and MITCHELL A. C., *Phys. Rev. B*, **59** (1999) 3434.
- [15] NELLIS W. J., *Sci. Am.*, **May** (2000) 60.
- [16] NELLIS W. J., MITCHELL A. C., MCCANDLESS P. C., ERSKINE D. J., and WEIR S. T., *Phys. Rev. Lett.* **68** (1992) 2937.
- [17] NELLIS W. J., MITCHELL A. C., VAN THIEL M., DEVINE G. J., TRAINOR R. J., and BROWN N., *J. Chem. Phys.* **79** (1983) 1480.
- [18] HOLMES N. C., ROSS M., and NELLIS W. J., *Phys. Rev. B* **52** (1995) 15,835.
- [19] BASTEA M., MITCHELL A. C., and NELLIS W. J., *Phys. Rev. Lett.*, **86** (2001) 3108.
- [20] Chau R. et al., to be published.
- [21] CHAU R., MITCHELL A. C., MINICH, R., and NELLIS W. J., *J. Chem. Phys.*, **114** (2001) 1361.
- [22] REE F. H., *J. Chem. Phys.*, **70** (1979) 974.
- [23] NELLIS W. J., HAMILTON D. C., and MITCHELL A. C., *J. Chem. Phys.*, **115** (2001) (in press)

- [24] WEIR S. T., MITCHELL A. C., and NELLIS W. J., *J. Appl. Phys.*, **80** (1996) 1522.
- [25] FUNAMORI N. and JEANLOZ R., *Science* **278** (1997) 1109.
- [26] TERNOVOI V. Ya, et al, *Physica B*, **265** (1999) 6.
- [27] R. Minich, (private communication).
- [28] KERLEY G. I., in *Molecular-Based Study of Fluids*, edited by J. M. Haile and G. A. Mansoori (American Chemical Society, Washington) 1983, pp. 107-138.
- [29] ROSS M., *Phys. Rev. B*, **58** (1998) 669.
- [30] LENOSKY T. J., KRESS J. D., COLLINS L. A., and KWON I., *Phys. Rev. B*, **55** (1997) R11907.
- [31] ASHCROFT N. W., *Phys. Rev. Lett.*, **21** (1968) 1748.
- [32] HENSEL F. and EDWARDS P., *Phys. World*, **4** (1996) 43.
- [33] HERZFELD K. F., *Phys. Rev.*, **29** (1927) 701.
- [34] IOFFE A. F. and REGAL A. R., *Prog. Semicond.*, **4** (1960) 237.
- [35] NELLIS W. J., LOUIS A. A., and ASHCROFT N. W., *Philos. Trans. R. Soc. London, Ser. A*, **356** (1998) 119.
- [36] KRESS J., COLLINS L., LENOSKY T., KWON I., and TROULLIER N., in *Strongly Coupled Coulomb Systems*, edited by G. J. Kalman, J. M. Rommel, and K. Blagoev (Plenum, New York) 1998, pp. 331-335.
- [37] NELLIS W. J., this proceedings.
- [38] ROSS M., REE F. H., and YOUNG D. A., *J. Chem. Phys.*, **79** (1983) 1487.
- [39] MITCHELL A. C. and NELLIS W. J., *J. Chem. Phys.*, **76** (1982) 6273.
- [40] CHAU R., MITCHELL A. C., MINICH R. W., and NELLIS W. J., *J. Chem. Phys.* **114** (2001) 1361.
- [41] HAMANN S. D. and LINTON M., *Trans. Faraday Soc.*, **62** (1966) 2234.
- [42] CAVEZZONI C., CHIOROTTI G. L., SCANDOLO S., TOSSATI E., M. BERNASCONI M., and PARRINELLO M., *Science*, **283** (43)43]1999) 44.
- [43] MITCHELL A. C., SHANER J. W., and KEELER R. N., *Physica*, **139&140** (1986) 386

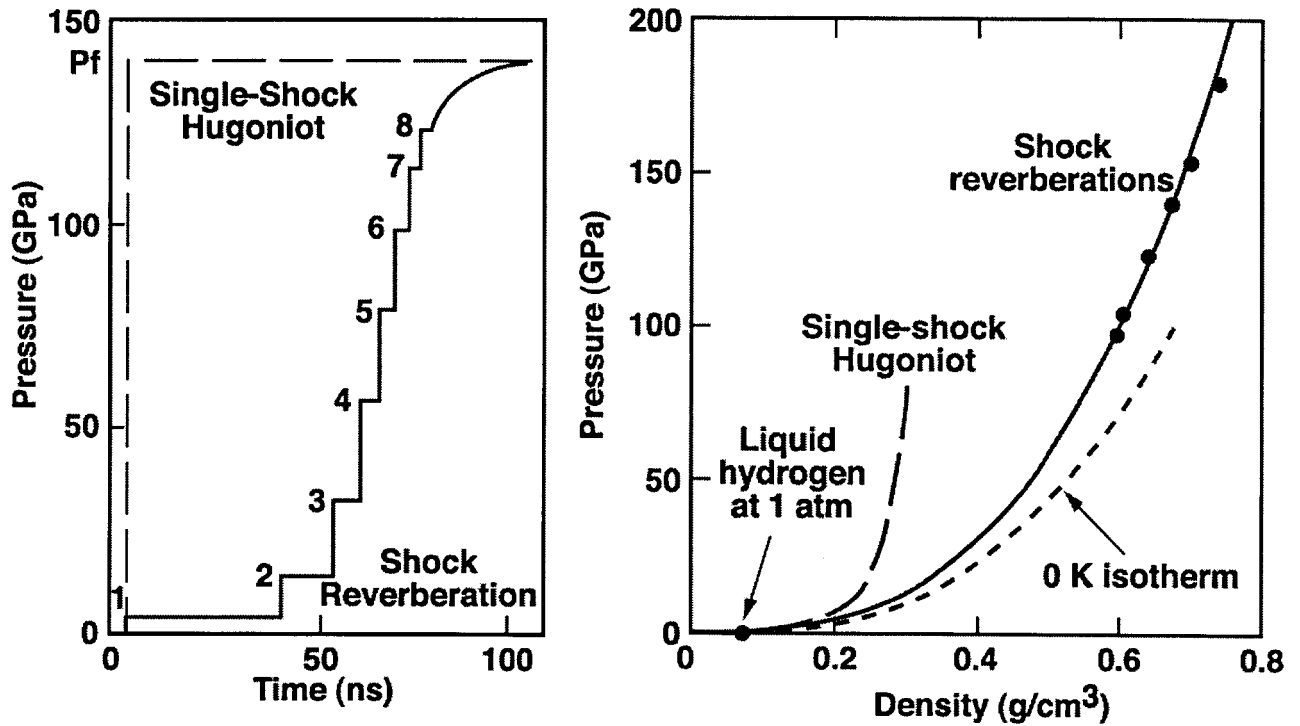


Fig. 1. Schematic illustration of effect of time interval over which pressure is applied on thermodynamic states achieved. One strong shock on Hugoniot produces high thermal and total pressures (long-dashed curve). Series of many shocks produces substantially lower temperatures and thermal pressures and substantially higher densities (solid curve) close to 0-K isotherm (short-dashed curve) [14].

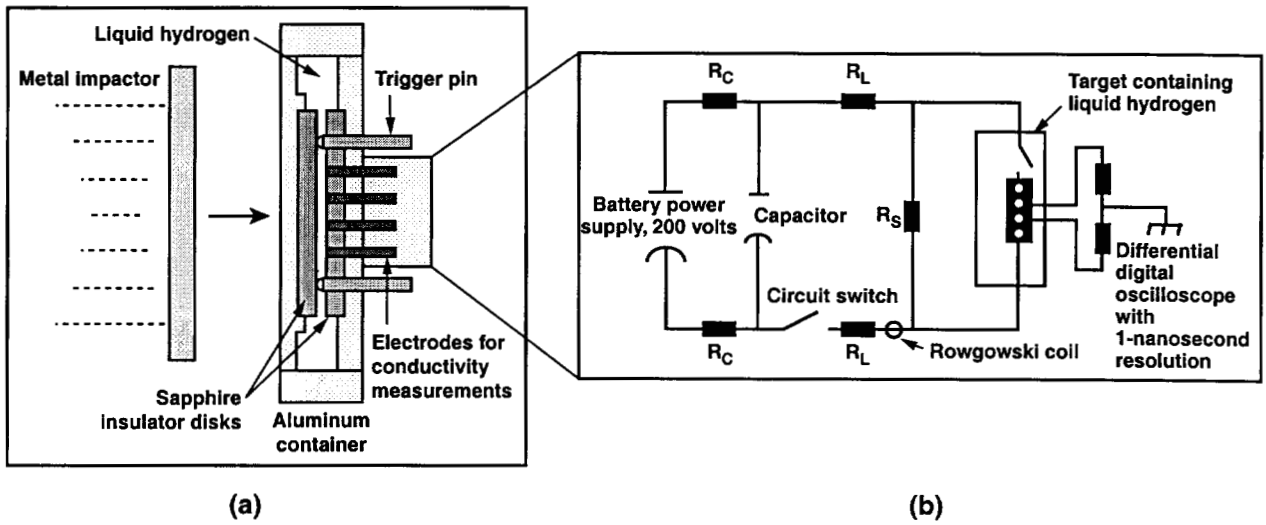


Fig. 2. Schematic of electrical conductivity experiments. Four electrodes in (a) were connected to circuit in (b). Metal impactor is accelerated to ~ 7 km/s with two-stage light-gas gun [14].

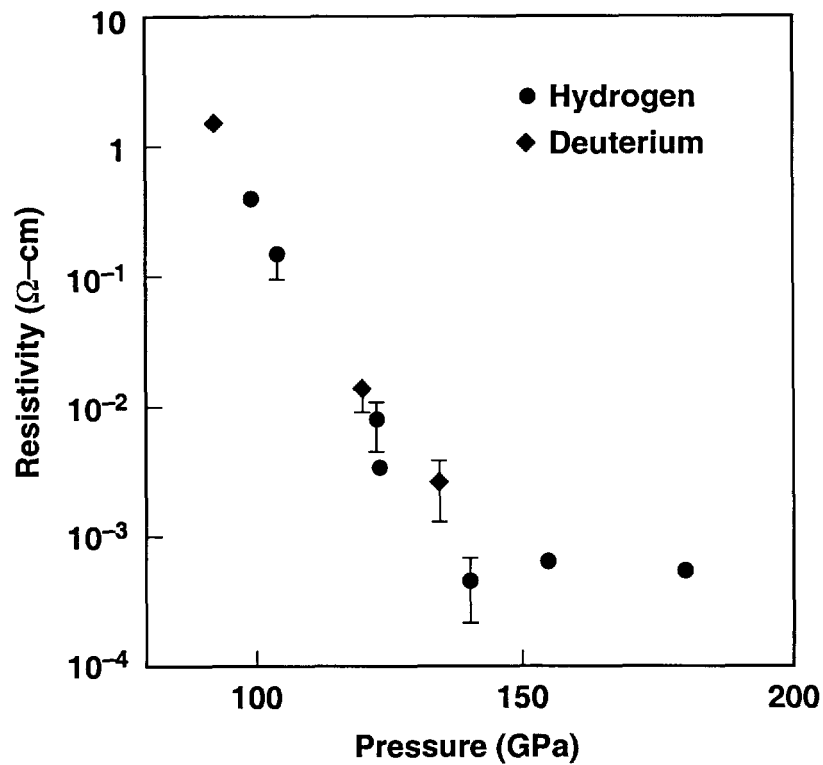


Fig. 3. Logarithm of measured electrical resistivities of H_2 and D_2 plotted versus pressure. Pressure is maximum pressure, P_F in Fig. 4, achieved by shock reverberating in hydrogen between two sapphire anvils in Fig. 2. Two isotopes are used to vary densities and temperatures. There is no isotope effect at these temperatures [14].

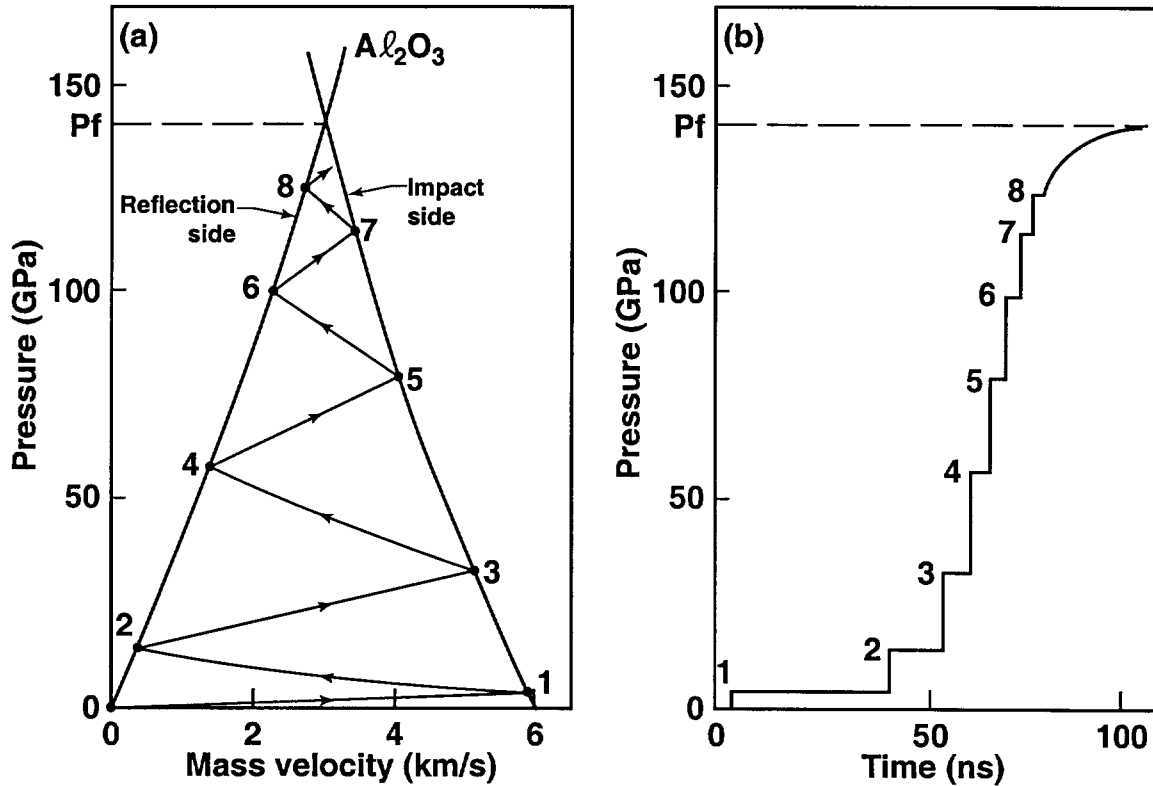


Fig. 4 . Shock reverberation in hydrogen. These curves were calculated [27] for 140 GPa. (a) Pressure P versus mass velocity u_p . Reflection side is sapphire on right and impact side is sapphire on left in Fig. 2a. State 1 is first shock in hydrogen; state 2 is reached when first shock reflects off Al_2O_3 on right in Fig. 1a; etc. Even-numbered (P , u_p) states lie on Al_2O_3 Hugoniot; odd-numbered states lie on mirror reflection of Al_2O_3 Hugoniot. (b) Pressure versus time t at midpoint of hydrogen layer. State 1 is shock; states 2 and higher are very weak shocks and comprise a quasi-isentrope. P_f is final pressure in hydrogen, equal to pressure incident from sapphire on left. Thermal equilibrium is achieved within thickness of indicated risetime of each step [14].

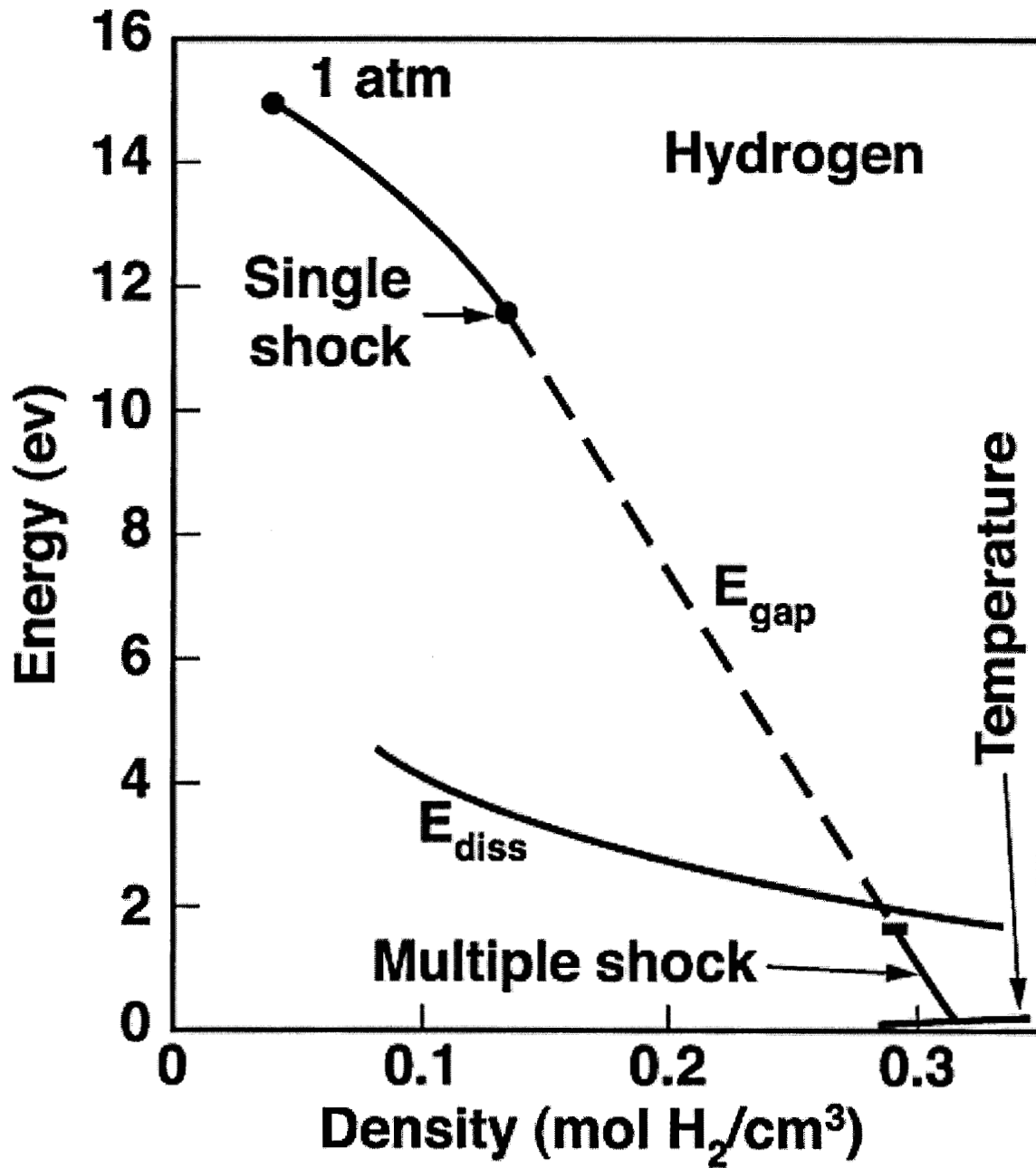


Fig. 5. Characteristic energies plotted versus molar density, assuming hydrogen is molecular: electronic mobility gap E_{gap} , molecular dissociation energy E_{diss} extrapolated from [18], and calculated temperatures $k_B T$ [14].

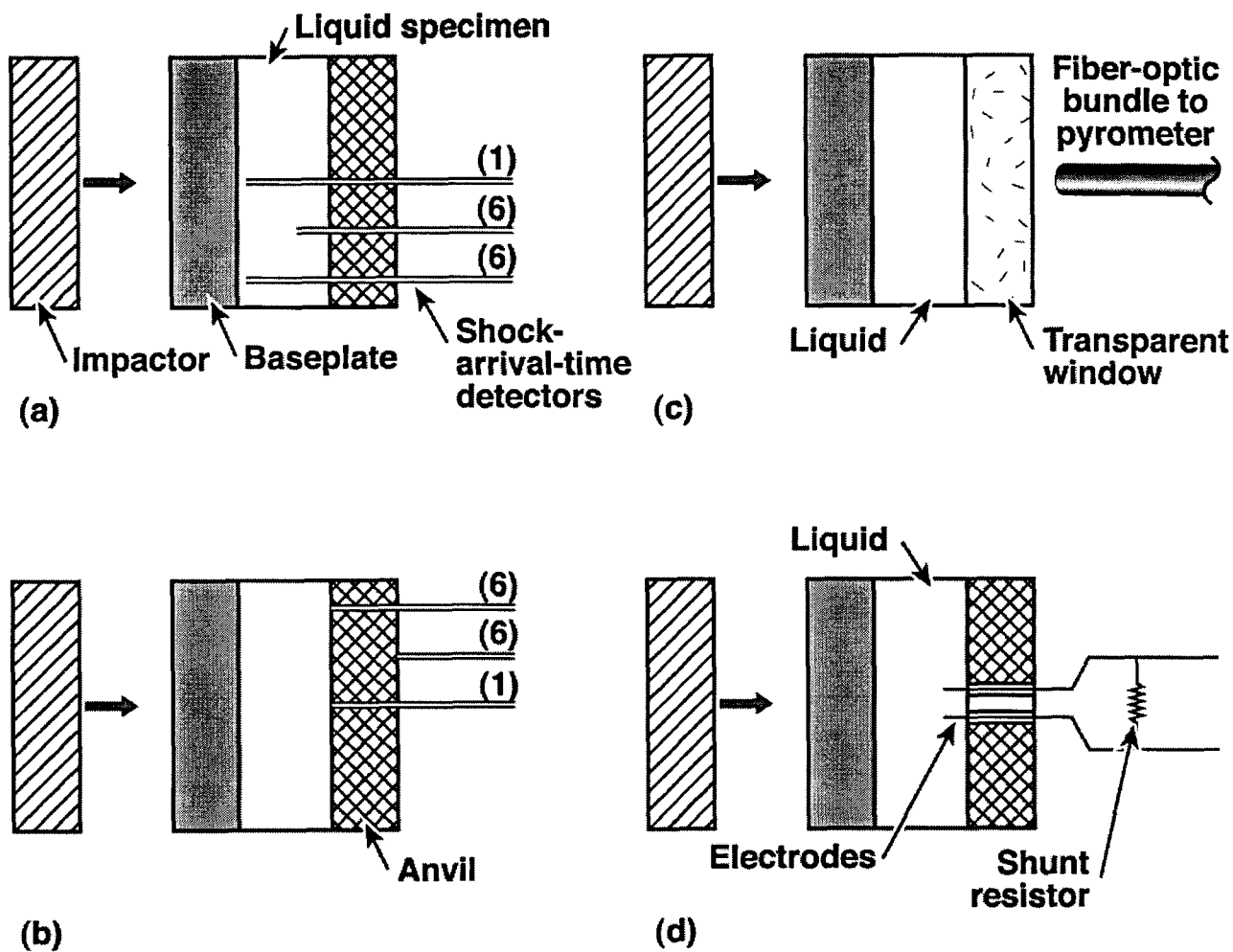


Fig. 6. Schematics of (a) Single-shock Hugoniot EOS experiment. Six detectors are positioned in liquid on each of two levels with a central detector on axis. (b) Double-shock Hugoniot EOS experiment. Detectors are arrayed to measure shock velocity across anvil. (c) Optical shock temperature experiment under single and double -shock compression. (d) Electrical conductivity experiment under single-shock compression.

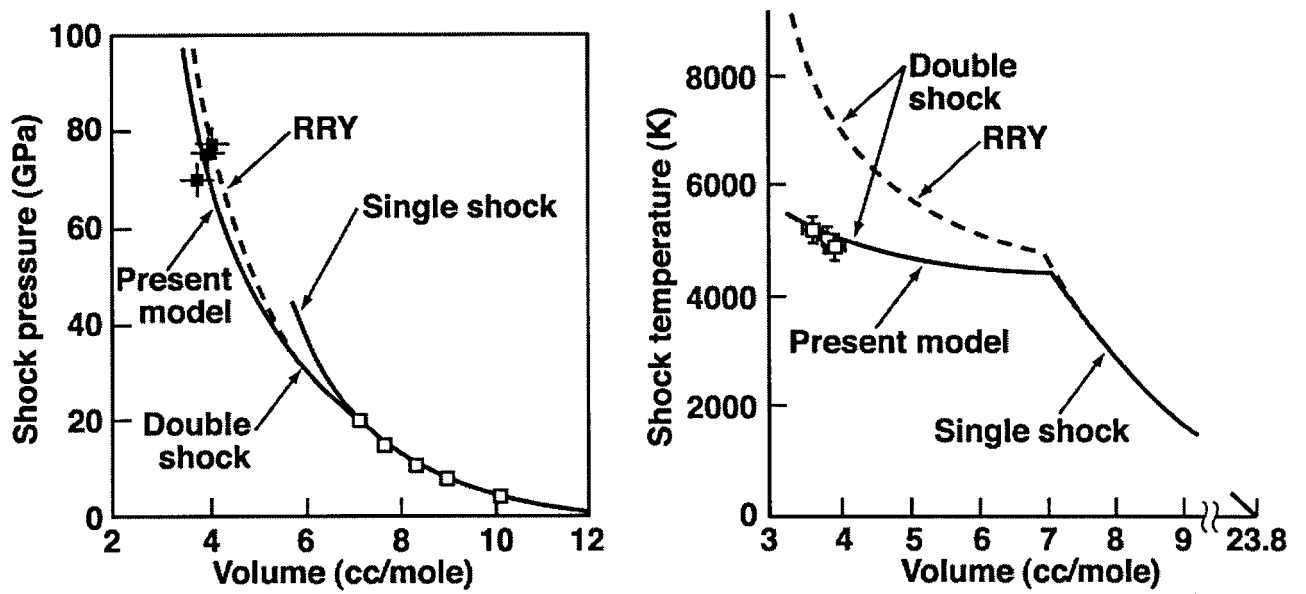


Fig. 7. Single and double-shock EOS data for liquid D_2 [17,18]. On the left are Hugoniot pressure-volume data (Figs. (6a) and (6b)) [17]; on the right are temperature data (Fig. (6c) [18]. Present model is in [18]; RRY is [38].

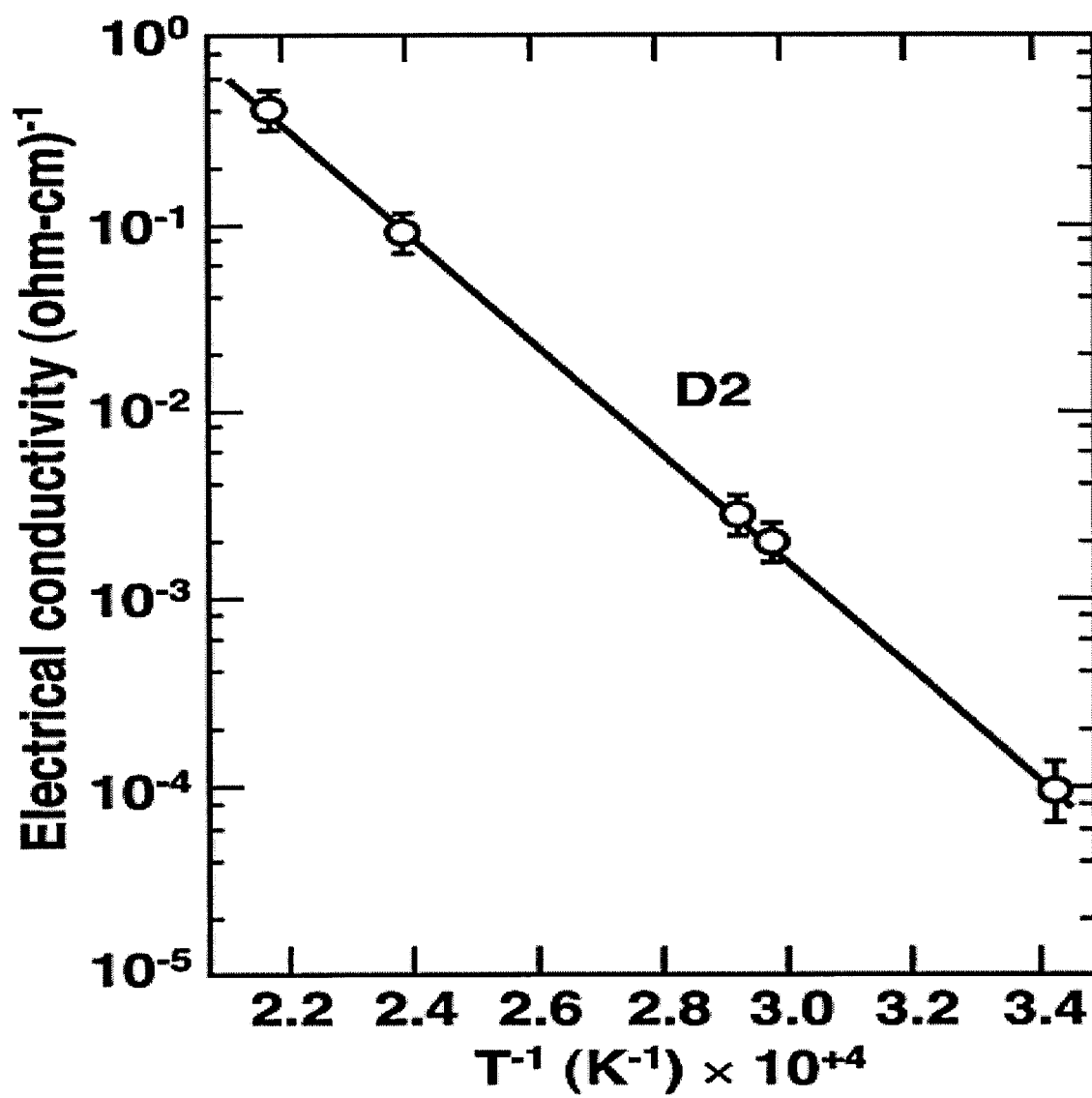


Fig. 8. Lagarithm of electrical conductivity of shock-compressed liquid D_2 versus reciprocal shock temperature [16].

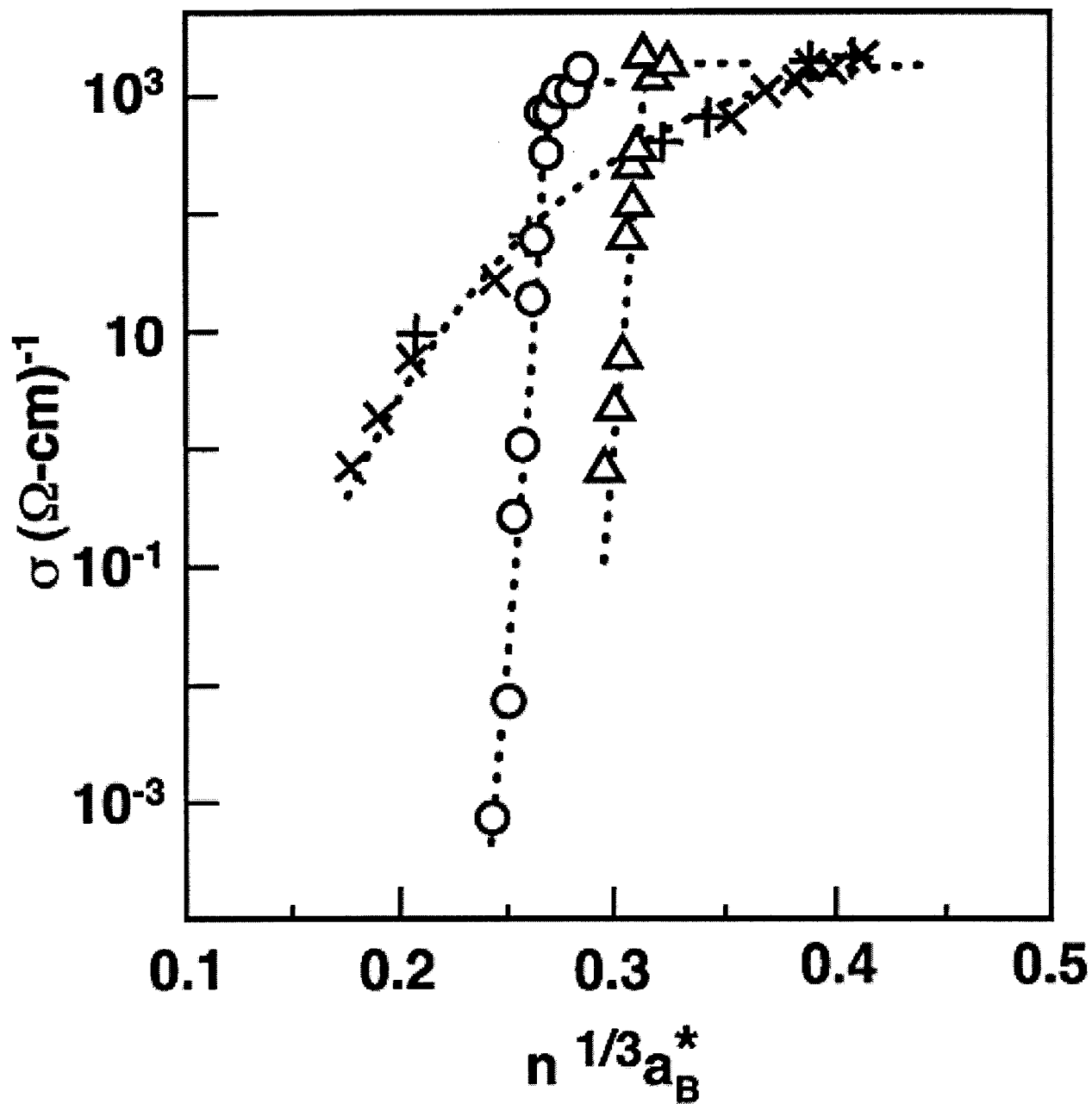


Fig. 9. Electrical conductivities versus Mott scaling parameter for oxygen (circles), hydrogen (triangles), rubidium (crosses), and cesium (x). Dotted lines are guides to the eye [19].

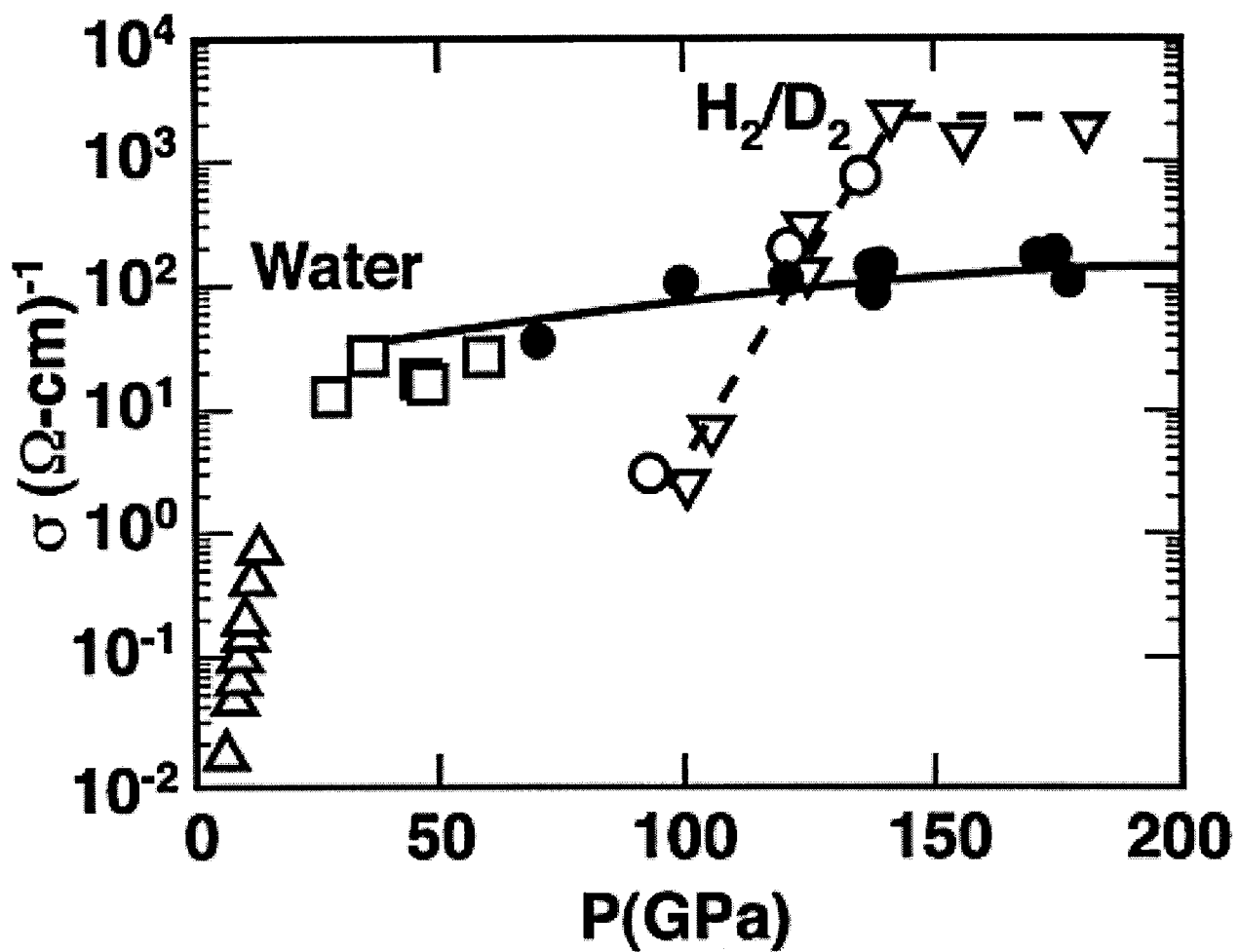


Fig. 10. Electrical conductivities of water and hydrogen plotted versus shock pressure. Triangles are [41]; squares are [39]; and solid circles are [40]. Open circles and inverted triangles are [14].

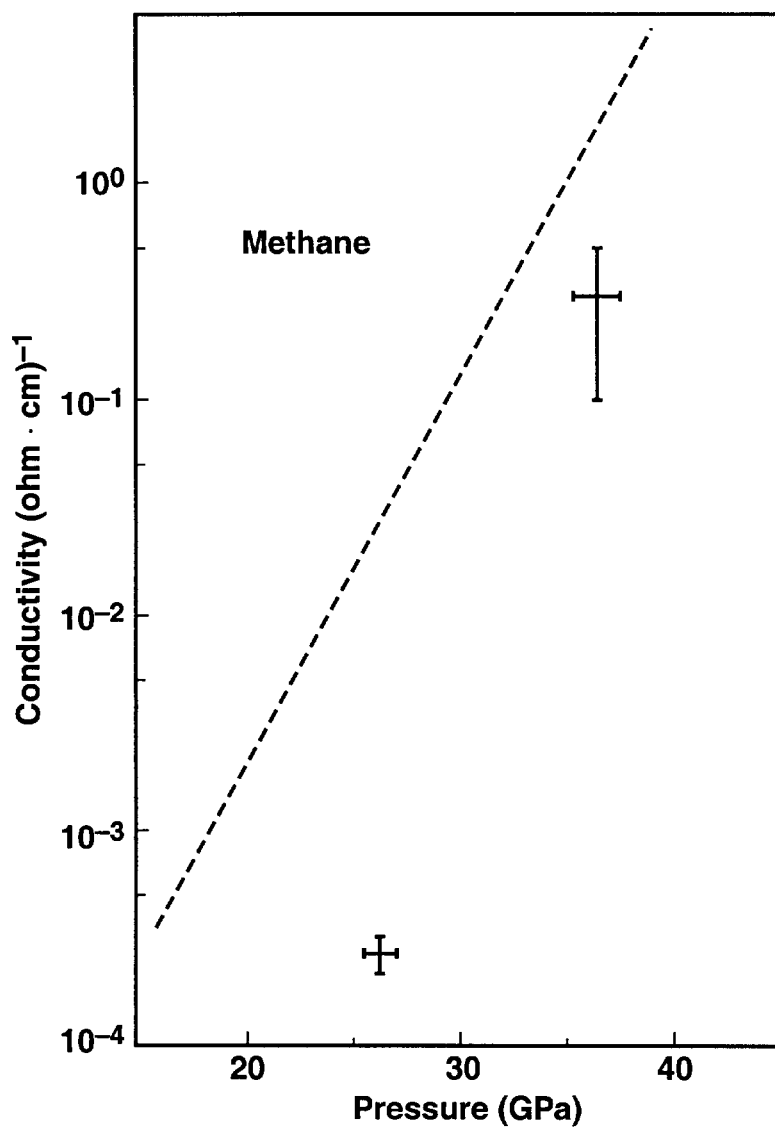


Fig. 11. Electrical conductivity of methane versus shock pressure. Crosses are data points; dashed line is calculated assuming electrical conduction is only through fluid H₂ formed on decomposition of methane into H₂ and diamond-like C nanoparticles [44].

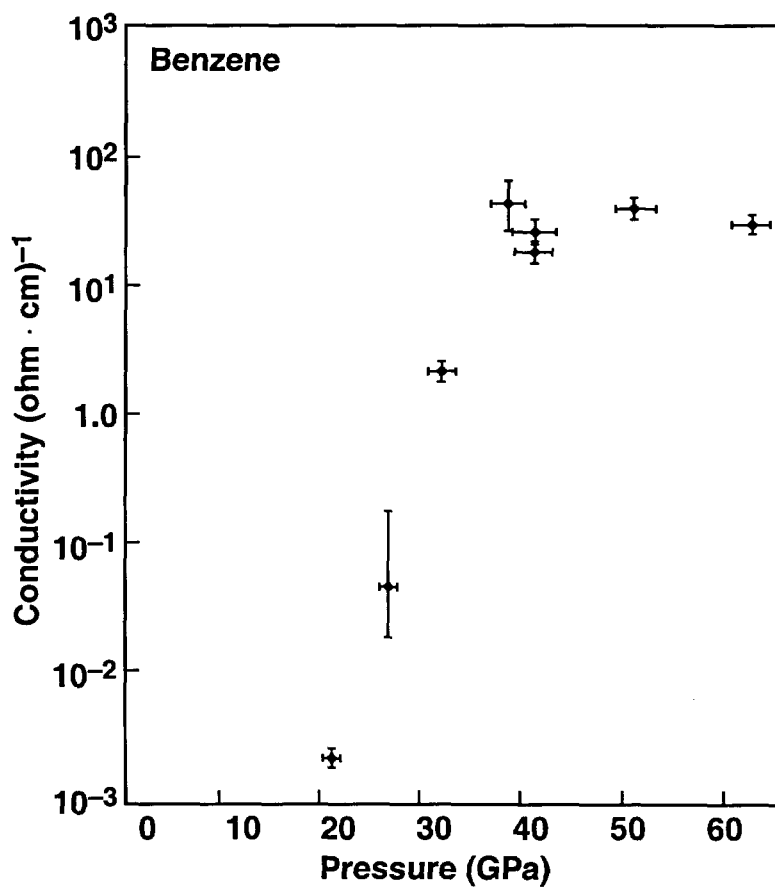


Fig. 12. Measured electrical conductivities of benzene vs shock pressure. Conductivity saturates at ~ 40 (ohm-cm)⁻¹. 40 GPa occurs at a critical density at which connectivity of C nanoparticles becomes sufficiently large that further increase in density has weak affect on the effective cross sectional area for electrical conduction [44].